International Journal of Multiphase Flow 35 (2009) 389–397

Contents lists available at ScienceDirect

International Journal of Multiphase Flow

journal homepage: www.elsevier.com/locate/ijmulflow

Critical friction factor modeling of horizontal annular base film thickness

D. Schubring, T.A. Shedd *

Multiphase Flow Visualization and Analysis Laboratory, University of Wisconsin-Madison, 1500 Engineering Drive, Madison, WI 53706-1609, USA

ARTICLE INFO

Article history:
Received 24 September 2008
Accepted 8 December 2008
Available online 12 January 2009

Keywords:
Air–water
Film thickness
Horizontal flow
Annular flow
Critical film flow rate

ABSTRACT

Measurements of liquid base film thickness distribution have been obtained for 206 horizontal annular two-phase (air–water) flow conditions in 8.8 mm, 15.1 mm, and 26.3 mm ID tubes. It is found that the trends in base film thickness measurement do not match trends in the literature for average film thickness, which considers waves and base film together. An iterative critical friction factor model is used to model circumferentially-averaged base film thickness; an explicit, empirical correlation is also provided. Asymmetry is well-correlated by a modified Froude number based on the correlated base film thickness and the gas mass flux. The iterative model is also extended to estimate the critical film flow rate.

1. Introduction

In two-phase annular flow, many behaviors are thought to be linked to film thickness, the size of the thin layer of liquid around the periphery of the tube. Correlations for interfacial shear, which are used as a step towards modeling frictional pressure loss, have required film thickness or closely related data since the formative work of Wallis (1969). The excess liquid concept, advanced by Schadel (1988) and others, requires knowledge of the film flow rate as separate from liquid flow in entrained droplets. A detailed understanding of film behavior, including film thickness and turbulence information, is also prerequisite for a plausible mechanistic model of heat transfer.

Hewitt et al. (1990) observed that this film is composed of a relatively smooth region (base film) and disturbance waves. The recent model of Hurlburt et al. (2006) was one of the first to consider these two zones separately with regard to interfacial shear and pressure loss. In that model, a statistical criterion was used to separate base film from waves, with film thickness measured by conductance probes.

In the present work, an optical film thickness measurement technique was selected (as outlined by Shedd and Newell (1998) and further verified by Rodríguez and Shedd (2004)) that directly provides indication of the base film thickness. In addition, pressure drop and wave measurements were taken; these have been discussed in more detail in other works (Schubring and Shedd, 2008, 2009, respectively). These works have shown that published film roughness correlations do not perform well for the present databank when base film thickness is used. This indicates that consideration of wave behavior is necessary, either through wave height and intermittency, as in average film thickness, or the gas friction velocity.

Most often, average film thickness is taken as an experimental input to a model, complicating analysis, as film thickness measurements can be quite challenging to perform. Conductance probes do not differentiate between disturbance waves and base film thickness, may not entirely eliminate the effect of entrained droplets in the gas core or bubbles in the film, are invasive into the experiment, and require careful calibration. Optical methods, such as those used in the present study, require calibration and a clear tube for visualization. Further, in the case of horizontal flow, a single measurement of film thickness is not sufficient. Instead, several measurements must be taken to study the distribution of liquid around the tube.

Many authors have attempted to model this film thickness distribution. Similar outlines of the physics suggested are provided by Sutharshan et al. (1995) and Jayanti et al. (1990). One of the early hypotheses, promoted by the work of Pletcher and McManus (1965) and refined quantitatively by Laurinat et al. (1985) and Lin et al. (1985), was that the asymmetry produces a circumferential variation in interfacial roughness that produces a two-vortex secondary flow in the gas core, driving liquid up the tube wall. An entrainment-centric model was suggested by research culminating in a paper by Anderson and Russell (1970). This model was also explored by later authors and helped to spur work on droplet deposition. A wave-spreading mechanism was proposed by Butterworth (1972). The model of Fukano and Ousaka (1989) applied a wave pumping mechanism. Aware of the models above, Jayanti et al. (1990) recommended a wave-inclination model instead, citing differences in wave behavior between the bottom and top of the tube. Their data are at somewhat lower gas flow rates than those in the present study. Sutharshan et al. (1995) pro-

* Corresponding author. Tel.: +1 608 265 2930; fax: +1 608 262 8464.
E-mail address: shedd@engr.wisc.edu (T.A. Shedd).

0301-9322/$ - see front matter © 2009 Elsevier Ltd. All rights reserved.
doi:10.1016/j.ijmultiphaseflow.2008.12.002

duced experimental data consistent with the hypothesis of Fukano and Ousaka but suggest further work is necessary for refinement. The data range in that work overlaps with the current set. More recent work by Hurlburt and Newell (2000) simplified Laurinat's model and showed that it was a good fit for a wide range of horizontal average film thickness data.

All of these analyses consider the distribution of average film thickness, rather than base film alone. The present work provides two relations for average base film thickness based on a large databank of air–water data in small diameter horizontal tubes. The first is a model based on a critical friction factor. However, it requires iteration, so a second, purely empirical relation is provided. A simple asymmetry correlation is also provided.

2. Experimental setup

2.1. Flow loop

The two-phase flow loop used for these experiments is shown in Fig. 1. Laboratory compressed air was delivered to the test section inlet via a bank of variable-area volumetric flow meters. The uncertainties, based on manufacturer's stated values and including density correction, were 8.4 L min^{-1} below 250 L min^{-1} flow, 14 L min^{-1} between 300 and 700 L min^{-1} flow, and 68 L min^{-1} above 700 LPM L min^{-1} flow. A pressure gauge near the flow meters allowed for the correction of flow meter readings to compensate for variations in air density and for the calculation of the mass flow rate entering the test section. Water entered the flow loop through a series of small (1.5 or 3 mm) holes drilled in the test section wall about 150 mm from the air entrance.

The two-phase air/water mixture passed through a flow development length before any measurements were obtained. This length was 400 diameters for the 8.8 mm ID tube, 330 diameters for the 15.1 mm ID tube, and 210 diameters for the 26.3 mm ID tube. (See Okada and Fujita (1990) for a discussion of required development length and the effects of the method of liquid introduction.) The air and water were separated in a gravity-assisted centrifugal separator, after which the water entered a holding reservoir. A variable-speed peristaltic pump was used to draw water from the reservoir through a 40 μm filter. Because of the pulsating nature of peristaltic pumps, a pulse dampening closed reservoir was placed after the pump. The liquid flow was measured using a bank of variable-area rotameters with manufacturer's specified accuracies of 45 cm^3 min^{-1} for less than 1500 cm^3 min^{-1} flow, 90 cm^3 min^{-1} for 1500–3000 cm^3 min^{-1} flow, and 5% of reading for above 3000 cm^3 min^{-1} flow. The test sections were constructed of clear PVC (Excelon R4000) for complete visualization of the flow from liquid entrance to exit.

2.2. Pressure measurement

A bourdon-tube gauge was placed near the test section to estimate local air density. In the 15.1 mm and 26.3 mm ID tubes, this gauge was placed at the beginning of the test section, while it was placed 0.5 m upstream for the 8.8 mm ID tube. The 8.8 mm ID case is shown in Fig. 1.

Using the two static pressure measurements, dry air mass was conserved in calculations. The air entering the test section was assumed to be dry at a temperature of 20 °C. Within the test section, a relative humidity of 100% was assumed at a temperature of 11 °C.

2.3. Film thickness measurement

Using a technique outlined by Shedd and Newell (1998), base film thickness measurements were made at the top, bottom, and side of the tube for each flow condition. This non-intrusive method uses the pattern of diffuse light reflected from the liquid surface to determine the liquid film thickness (see Fig. 1). Rodríguez and Shedd (2004) have shown, by comparisons with direct

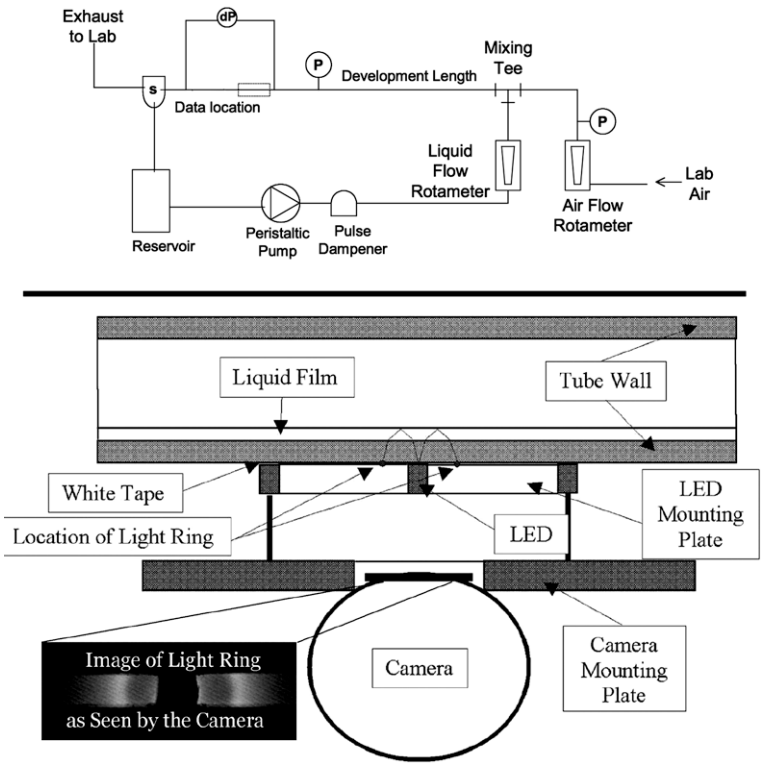

Fig. 1. (Top) Diagram of flow loop. (Bottom) Film thickness data acquisition system.

film measurements using planar fluorescence imaging, that this optical method accurately determines the mean film thickness between large liquid waves. Uncertainties vary with the film thickness and surface roughness (waviness). Uncertainties are estimated at 5–10% (highest for lowest gas flow rates). A calibration (bias) uncertainty of 5% is included in this estimate. This calibration will affect each measurement for a specific diameter and location (top, side, bottom).

The circumferentially-averaged base film thickness and maximum asymmetry were calculated by:

$$\delta = \frac{\delta_t + 2\delta_s + \delta_b}{4} \tag{1}$$

$$Assym = \frac{\delta_b}{\delta_t} \tag{2}$$

2.4. Data range

For each diameter, an array of meter readings was selected to provide a large bank of data. The 206 fully annular data points are a subset of this data. Superficial gas and liquid velocities were calculated according to Eqs. (3) and (4), with gas kinetic energy calculated according to Eq. (5). In these equations, G is the mass flux, x is the flow quality, $\dot{m}$ is a mass flow rate, KE_{sg} is the gas kinetic energy density (or dynamic pressure) based on superficial gas velocity, ρ is a density, and A refers to total flow area.

$$u_{sg} = \frac{Gx}{\rho_g} \tag{3}$$

$$u_{sl} = \frac{G(1-x)}{\rho_l} \tag{4}$$

$$KE_{sg} = \frac{U_{sg}^2 \rho_g}{2} \tag{5}$$

$$x = \frac{\dot{m}_g}{\dot{m}_g + \dot{m}_l} \tag{6}$$

$$G = \frac{\dot{m}_g + \dot{m}_l}{A} \tag{7}$$

Superficial gas velocities of between 28 and 86 m s^{-1} were considered, with superficial liquid velocities between 0.045 and 0.30 m s^{-1}. Flow qualities ranged from 0.12 to 0.78. Superficial gas kinetic energy densities ranged from 600 to 5400 J m^{-3} as a result of the variable superficial velocities and gas densities through the test section. The cut-off of 600 J m^{-3} was selected to correspond with a change in trends of pressure drop, film thickness distribution, and wave behavior that may be indicative of a transition from the fully annular behavior studied presently and a separate wavy-annular regime. The data included can be seen in Schubring and Shedd (2009) as arrays of G, x, and P.

3. Data and observation of trends

The data are shown in Fig. 2, which shows average base film thickness for all tubes, and Fig. 3, which shows the maximum asymmetry.

The following general trends are seen in these graphs:

- Average base film thickness is inversely related to gas flow rate (superficial velocity) at constant liquid flow rate.
- For high gas flow rates, the dependence of average base film thickness on liquid flow rate vanishes.
- The average base film thickness is larger for the larger tube diameters; however, the dependence is less than linear.
- The film becomes more symmetric as the gas flow rate increases.
- The dependence of asymmetry on liquid flow rate is small and becomes negligible for high gas flows.
- Asymmetry is more pronounced for larger tubes. Further, the dependence on liquid flow rate for lower gas flows is clearer for larger tubes.

Examination of the top, side, and bottom film thickness data also shows that, for fully annular flows, the side film thickness is very similar to the average. Therefore, modeling of the asymmetry of fully annular flow is well-approximated by a single parameter: the ratio of bottom and top base film thicknesses.

4. Average base film thickness

4.1. Empirical correlation

A first approximation to a film thickness correlation is shown in Eq. (8). This estimate entirely ignores the liquid flow; regardless, it provides agreement to within 11% MAE (defined by Eq. (9)) for the present data. Because an approximate expression is available so readily, a realistic model that includes the effects of both gas and liquid can be expected to provide excellent accuracy.

$$\delta = 12.5 D Re_{gas}^{-\frac{2}{3}} \tag{8}$$

$$MAE = \frac{1}{n}\sum_{i=1}^{n}\left|\frac{x_{corr,i} - x_{exp,i}}{x_{exp,i}}\right| 100\% \tag{9}$$

The purely empirical correlation shown in Eq. (10) produces comparable statistics (MAE, RMS, etc.) as the critical friction factor model (below) for the current databank. It includes effects of liquid flow (through quality and a liquid Reynolds number – Eq. (11)) as well as a dependence on gas density. However, the authors advise against extending this relation beyond the specific range of conditions in the present study, as it was constructed using trial and error and dimensional analysis.

$$\frac{\delta}{D} = 4.7\frac{1}{x}\left(\frac{\rho_g}{\rho_l}\right)^{\frac{1}{3}} Re_G^{-\frac{2}{3}} \tag{10}$$

$$Re_G = \frac{GD}{\mu_l} \tag{11}$$

4.2. Critical friction factor model

A common approach in the literature is to assume a critical Reynolds number in the film; however, the present data are poorly correlated by such an expression. Noting the strong dependence of both film thickness and single-phase friction factors on the gas Reynolds number, a critical friction factor hypothesis is proposed. For the Reynolds numbers seen in fully annular flow and relative roughness on the order of film thickness, it can be shown that both terms – roughness and gas Reynolds number – are significant in computing the total friction factor.

By computing a smooth-tube friction factor and a fully roughened wall friction factor, using a fraction of the base film thickness to model ripples on the base film as an approximation for sand roughness, it was found that the ratio of the two friction factors, termed ϕ_{RR} in the present model, varied over a relatively narrow range. Assuming that the ratio between these friction factors is fixed allows a film thickness to be calculated iteratively; this relation has comparable accuracy as Eq. (8). The friction factors selected for this model are the fully rough tube Haaland correlation (Eq. (12)) and the smooth tube McAdams correlation (Eq. (13)), increased by a constant factor ϕ_{RR}.

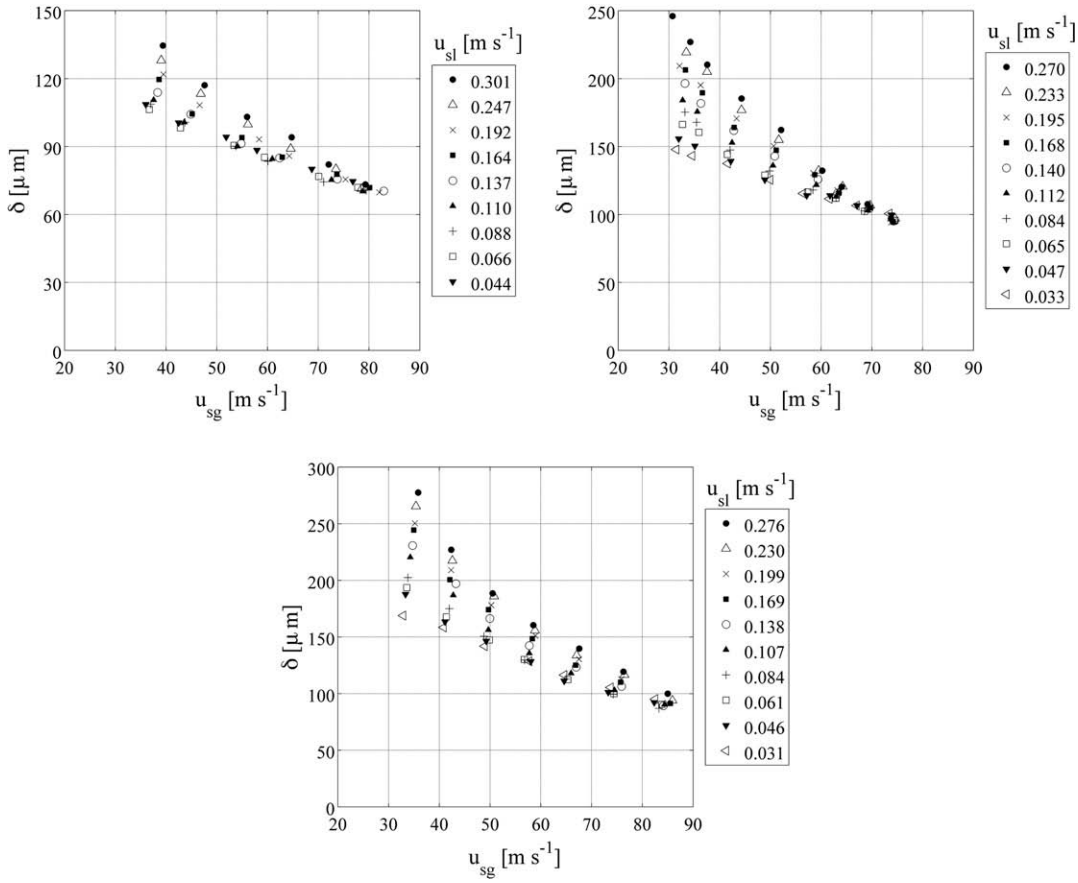

Fig. 2. Average base film thicknesses. (Top Left) 8.8 mm tube. (Top Right) 15.1 mm tube. (Bottom) 26.3 mm tube.

$$\frac{1}{\sqrt{f_{crit}}} = -1.8\, log_{10}\left[\frac{6.9}{Re_{shear}} + \left(\frac{RR_{crit}}{3.7}\right)^{\frac{10}{9}}\right] \tag{12}$$

$$f_{crit} = 0.184\phi_{RR} Re_{shear}^{-0.20} \tag{13}$$

By adjusting the Reynolds number used to consider the relative velocity of the gas core and the top of the film, as well as the diameter of the gas core (rather than the whole tube), improvement to 9% MAE is possible. If the size of ripples is taken as a weak function of flow quality, the present model, accurate to within 6% MAE, can be constructed. It is necessary to iterate on the core diameter, D_{core}, and shearing velocity, V_{shear}, to achieve convergence. These, along with the gas core shear Reynolds number, are defined by:

$$D_{core} = D - 2\delta \tag{14}$$

$$V_{shear} = V_g - V_{l,int} \tag{15}$$

$$Re_{shear} = \frac{\rho_g V_{shear} D_{core}}{\mu_g} \tag{16}$$

The velocity of the gas core, V_g, is found by:

$$A_g = \frac{\pi D_{core}^2}{4} \tag{17}$$

$$V_g = \frac{\dot{m}_g}{\rho_g A_g} \tag{18}$$

The gas-core roughness multiplier, ϕ_{RR}, is set based on experimental data and the details of the assumed velocity profile within the film. A dependence on wall–liquid interaction (hydrophobicity) may also exist. For the current air–water–PVC apparatus and the set of assumptions discussed below, the gas-core ϕ_{RR} was found to best correlate to 1.289. It is also found that averaging friction factors from the Haaland equation applied at the top, side, and bottom of the tube produces nearly identical results as solving for a single friction factor based on an average base film thickness. Since averaging friction factors complicates the model and couples an asymmetry calculation, it is recommended that an average base film thickness be used to calculate an effective friction factor.

The size of ripples, dy_{ripple}, is modeled by Eq. (19). This size is used to define the relative roughness, RR_{crit} (Eq. (20)). The weak dependence on quality is similar to the dependence on Re_{shear} in Eq. (13) and accounts for the disruptive effects of waves and droplets. Resulting relative roughness ranged from 0.001 to 0.004, based on ripple sizes between 18 and 57 μm (between 20% and 32% of the corresponding film thickness).

$$dy_{ripple} = \frac{\delta}{3} x^{0.25} \tag{19}$$

$$RR_{crit} = \frac{dy_{ripple}}{D_{core}} = \frac{\delta}{3D_{core}} x^{0.25} \tag{20}$$

A schematic of the base film is shown in Fig. 4 showing the assumed velocity profile (indicated by a line) as well as the fluid beneath ripples (darkly shaded) and the ripple region (lightly shaded). The δ^+_{mod} (defined below) of 10 and ripple size (5 in wall coordinates) shown are typical of the present model.

The velocity of the top of the film is calculated based on a linear profile using the modeled wall shear ($\tau_{w,mod}$) to determine the slope from the wall to the bottom of the ripples and constant (well-mixed) beyond this. Modeled interfacial shear, $\tau_{i,mod}$, is calculated based on f_{crit} (Eq. (21)) and is converted to wall shear ($\tau_{w,mod}$) according to Eqs. (22) and (23) with a self-consistent pressure gradient. This modeled wall shear, and corresponding pressure gradient, strongly underpredicts experimental data (see

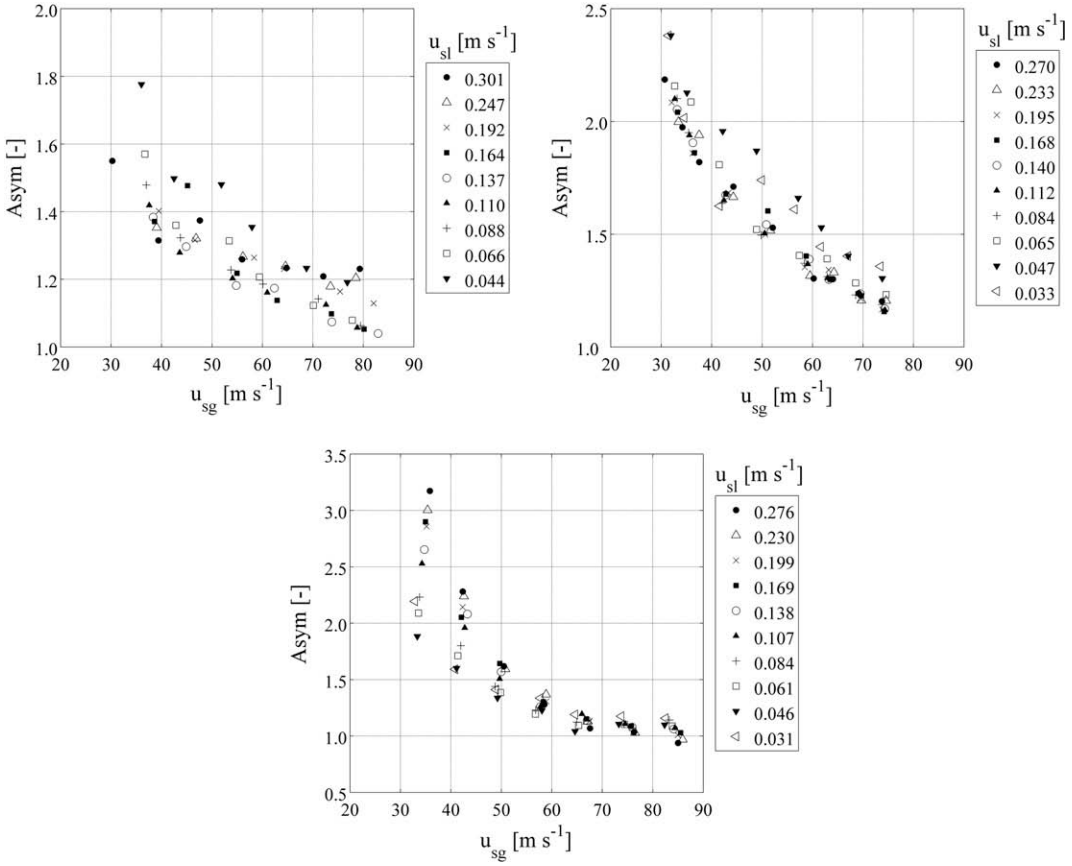

Fig. 3. Ratio of bottom to top base film thickness (asymmetry). (Top Left) 8.8 mm tube. (Top Right) 15.1 mm tube. (Bottom) 26.3 mm tube.

Schubring and Shedd, 2009) at high liquid flows, since waves and droplets (significant phenomena in these flows) are not considered.

$$\tau_{i,mod} = \frac{f_{crit}}{4}\frac{\rho_g V_{shear}^2}{2} \tag{21}$$

$$\tau_{i,mod} = -\frac{D_{core}}{4}\left(1 - \frac{\rho_g V_{shear}^2}{P}\right)\frac{dP}{dz} \tag{22}$$

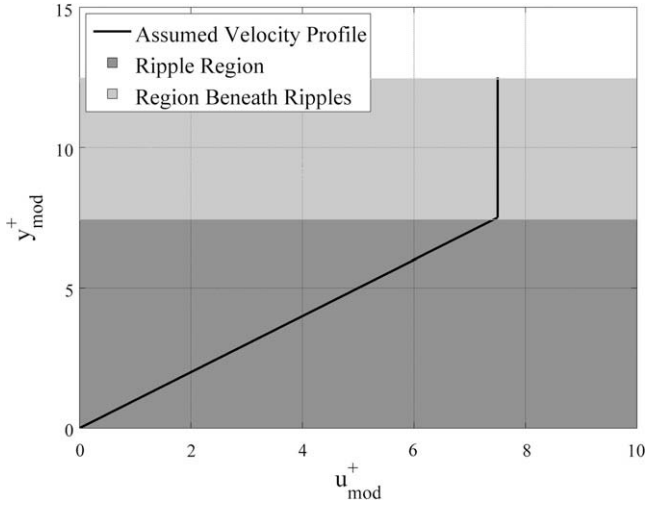

Fig. 4. Schematic of assumed ripple region and assumed velocity profile.

$$\tau_{w,mod} = \tau_{i,mod}\frac{D_{core}}{D} - \frac{1}{4}\frac{dP}{dz}\frac{D^2 - D_{core}^2}{D} \tag{23}$$

The velocity of the liquid at the interface is calculated according to the following equations. The fraction of the film modeled as linear (from the wall to the troughs of ripples) is referred to as the "linear fraction" (LF). The velocity above the troughs, assumed constant, is termed $u^+_{max,mod}$.

$$u^*_{mod} = \sqrt{\frac{\tau_{w,mod}}{\rho_l}} \tag{24}$$

$$\delta^+_{mod} = \frac{\delta u^*_{mod}}{\nu_l} \tag{25}$$

$$LF = \frac{\delta - 0.5dy_{ripple}}{\delta} = 1 - \frac{x^{0.25}}{6} \tag{26}$$

$$u^+_{max,mod} = LF\delta^+_{mod} \tag{27}$$

$$V_{l,int} = u^+_{max,mod}u^*_{mod} \tag{28}$$

The film thickness predictions of the present model are only weakly sensitive to the assumed velocity profile. Use of the universal velocity profile (UVP – Eq. (29), as presented by Whalley (1987)) alters the resulting MAE by less than 0.2%. Use of the UVP also changes the film flow rate results (discussed in Section 6.4) by less than 3% on average.

$$u^+ = \begin{cases} y^+ & \text{if } y^+ < 5 \\ -3 + 5\ln(y^+) & \text{if } 5 < y^+ < 30 \\ 5.5 + 2.5\ln(y^+) & \text{if } 30 < y^+ \end{cases} \tag{29}$$

A simple iteration scheme for these equations is to select an estimate for δ and $V_{l,int}$, perhaps 150 μm and 1 m s^{-1}, respectively. The film

thickness estimate can be used to calculate geometry, flow rates, and shear Reynolds number. The equality of the two expressions of friction factor based on this Reynolds number can then be used to update the estimate of roughness. An updated film thickness follows immediately. The velocity at the top of film can then be updated by calculating wall shear and using the velocity profile. This process can then be repeated until adequate convergence on δ is achieved.

5. Film thickness distribution

It was found that the asymmetry is best predicted by the ratio of gas mass flux (momentum density) and the square root of the predicted mean film thickness. This was expressed as a modified Froude number, Fr_δ (Eq. (30), where g is the acceleration due to gravity), to preserve a similar form as some of the literature (e.g., Hurlburt and Newell, 2000). An exponential curve, trending towards symmetry for high gas flow rates, was fit to the data (Eq. (31)). Predictions are made for local base film thickness by enforcing Eq. (1), applying the iterative friction factor model, using the asymmetry correlation presented here, and assuming that the side and average base film thicknesses are identical.

$$Fr_\delta = \frac{Gx}{\rho_l \sqrt{g\delta}} \tag{30}$$

$$Asym^{-1} = \frac{\delta_t}{\delta_b} = 1 - exp(-0.63 Fr_\delta) \tag{31}$$

6. Results and discussion

The results of the roughness-based model, along with the empirical equation (10), are shown in Fig. 5. The results for maximum asymmetry and top, side, and bottom film thicknesses are shown in Fig. 6. Results are also shown in Table 1 for average base film thickness, local base film thicknesses, and three measurements of asymmetry. The correlations presented are optimized such that mean errors are less than 1%. Beyond the strong statistical performance of the present model, there appears to be no trend to the residuals except at low gas flow rates for which the dependence of base film thickness on liquid flow rate is under-predicted.

6.1. Empiricism in iterative model

The model contains three empirical constants. The first is ϕ_{RR}, from Eq. (13). The others, the power on flow quality and the constant (one-third), are in Eq. (20), which relates film thickness and roughness. The constant factor was selected to agree with flow visualization, such as that of Rodríguez (2004), with consideration given to the observations discussed in Sections 6.3 and 6.4. It was observed that this constant could range from 0.1 to 1 with negligible change in MAE and other statistics, provided ϕ_{RR} was re-optimized; that is, the maximum ratio of ripple height to film thickness and ϕ_{RR} are not independent empiricisms for optimization of the model. Direct measurement of film roughness may remove the need for both the estimate of maximum ripple size and the quality dependence; this would leave only a single parameter, ϕ_{RR}, to be estimated from data.

6.2. Asymmetry

It was found that asymmetry in base film thickness is a weaker function of liquid flow rate than is average film thickness. Hurlburt and Newell (2000) suggest a correlation, of a similar form to Eq. (30), based on a modified Froude number:

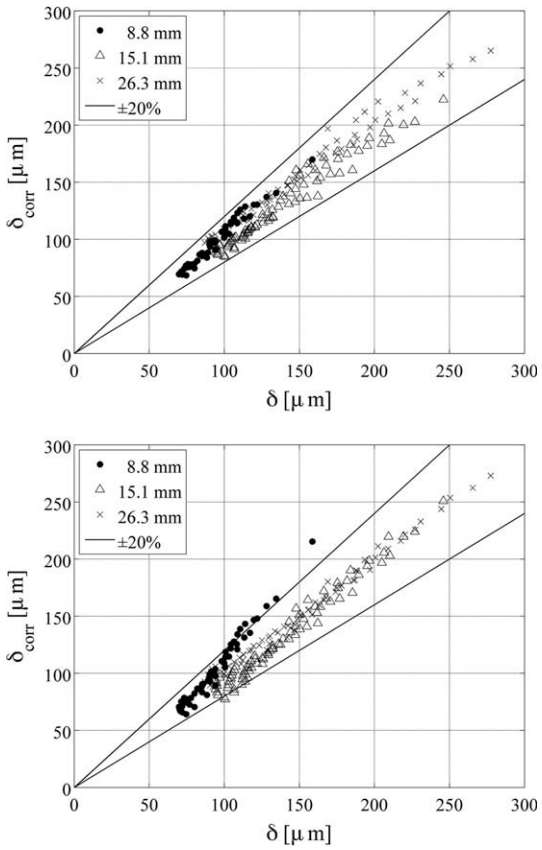

Fig. 5. (Top) Experimental average base film thickness vs. correlated average base film thickness, using iterative model. (Bottom) Experimental average base film thickness vs. correlated average base film thickness, using Eq. (10).

$$Fr_{H-N} = \frac{\dot{m}_g}{\dot{m}_l}\frac{U_{sg}^2}{gD} \tag{32}$$

Correlation to this dimensionless group was attempted for the present databank. It was found that this parameter overpredicts the diameter and liquid flow rate effects on asymmetry, with the liquid flow rate effect more strongly overpredicted.

If a correlation of asymmetry from this dimensionless group is accurate for average film thickness, this indicates that the asymmetry of waves and base film – the two parts of average film thickness – are not the same for the same flow condition and must be modeled independently. Correlation to Fr_{H-N} would indicate increasing asymmetry with increasing liquid flow, which is not seen in the present base film thickness data.

Since much of this increased liquid flow is transported by waves, this implies that waves are more asymmetric structures than is the base film. This implication emphasizes the differences in behavior between base film and waves and illuminates the challenges and limitations of mixing them into the average film thickness.

6.3. Estimate of wall shear

The model also produces estimates of wall shear (Eq. (23)) and liquid film flow rate ($\dot{m}_{lf}$ – Eq. (33)).

$$W_{mod}^+ = \int_0^{\delta_{mod}^+} u_{mod}^+ dy^+ = \delta_{mod^2}^+ \left[\frac{LF^2}{2} - (1-LF)LF\right] \tag{33}$$

$$\dot{m}_{lf} = W_{mod}^+ \pi D \mu_l \tag{34}$$

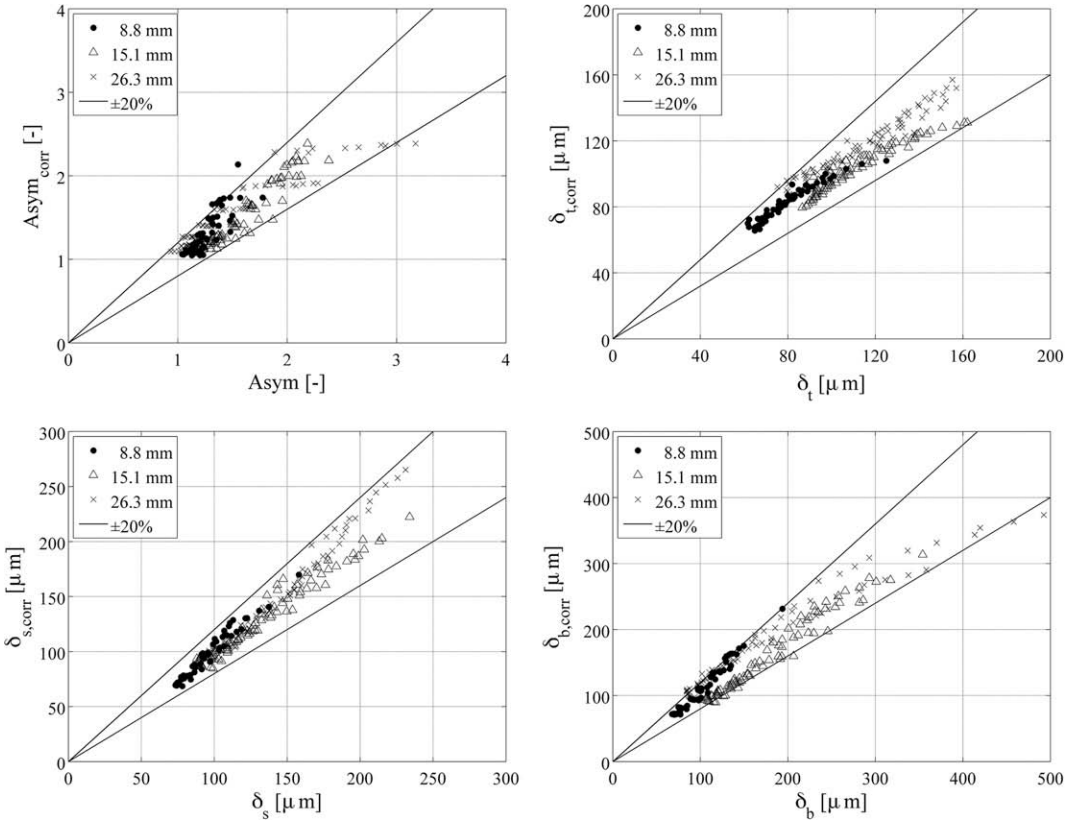

Fig. 6. Asymmetry and local base film thickness against correlations. (Top Left) Maximum asymmetry. (Top Right) Top base film thickness. (Bottom Left) Side base film thickness. (Bottom Right) Bottom base film thickness.

Table 1
Mean absolute (MAE) and root mean square (RMS) errors, present model.

Measurement	MAE (%)	RMS (%)
δ	5.67	6.82
δ_t	6.17	7.61
δ_s	5.17	6.51
δ_b	11.61	13.37
$\frac{\delta_b}{\delta_t}$	8.44	10.47
$\frac{\delta_s}{\delta_t}$	6.92	8.49
$\frac{\delta_b}{\delta_s}$	10.43	12.31

Fig. 7 shows the ratios of experimental wall shears (see Schubring and Shedd, 2009 for calculations) to those from the present model for the 15.1 mm tube. (The series in these plots are labeled by average gas superficial velocity, which varies by approximately 5% in a series; system pressure and gas density are also not constant within a series.) At low liquid flows, it is expected that the base film will transport the bulk of the liquid (i.e., few waves present to enhance shear), so only the base film model need be modeled to estimate shear. For low liquid flow conditions, reasonable agreement is found.

6.4. Low liquid flows – critical film flow rate

The present model is not appropriate at very low liquid flows; i.e., when the predicted film flow is larger than the total liquid flow. Fig. 7 shows the equivalent base film superficial velocity (that is, the superficial liquid velocity corresponding to $\dot{m}_{lf}$, referred to as $u_{s,film}$) as functions of actual liquid superficial velocity for the same series as the previous plot, again for the 15.1 mm tube. Extrapolating the trends, the equivalent base film superficial velocity appears to approach the actual liquid superficial velocity when the latter is between 1.2 and 1.6 cm s^{-1}, increasing with increasing gas flow.

These flow rates are below what could be measured accurately with the current experimental apparatus; however, a small number of film thickness measurements at liquid flows of 1.86 ± 20% cm s^{-1} were taken in the 15.1 mm tube. A 10–20% reduction in film thickness was found for high gas flows at this low liquid flow (relative to the fairly constant value at higher liquid flow and constant gas flow), along with an inability to detect waves with the apparatus discussed in Schubring and Shedd (2008). These results match what would be expected slightly below the critical film flow rate (the highest liquid flow rate for which 100% of the liquid is transported in the base film). No such reduction was seen at lower gas flows, matching the trends shown in Fig. 7 for critical film flow rate as a function of gas flow.

By iterating on $\dot{m}_l$ until convergence with $\dot{m}_{lf}$ is achieved, an estimate of this critical film flow rate ($\dot{m}_{crit}$) can be obtained using the critical friction factor model. The results from such a procedure are shown in Fig. 8. To preserve a similar form as that in the literature (e.g., Asali, 1984; Schadel, 1988), the values of $\dot{m}_{crit}$ are shown. These plots show that $\dot{m}_{crit}$ is a function of diameter, gas superficial velocity, and system pressure (through gas density). From these results, the power law proportionalities in Eq. (35) can be estimated:

$$\dot{m}_{crit} \propto \frac{D^{1.5} u_{sg}^{0.5}}{\rho_g^{0.6}} \tag{35}$$

The work of Schadel (1988) provides experimental results regarding liquid droplet entrainment. By extrapolating these data as functions of total liquid flow rate to the liquid flow corresponding to zero entrainment, an estimate of the critical liquid flow was obtained

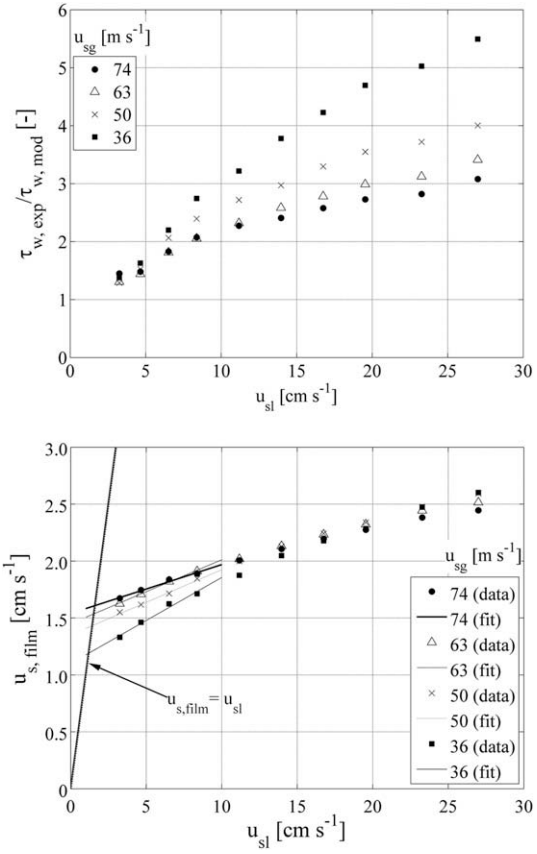

Fig. 7. Additional model outputs, 15.1 mm tube. (Top) Ratio of experimental wall shear to wall shear from the iterative friction factor model. (Bottom) Liquid film flow rate.

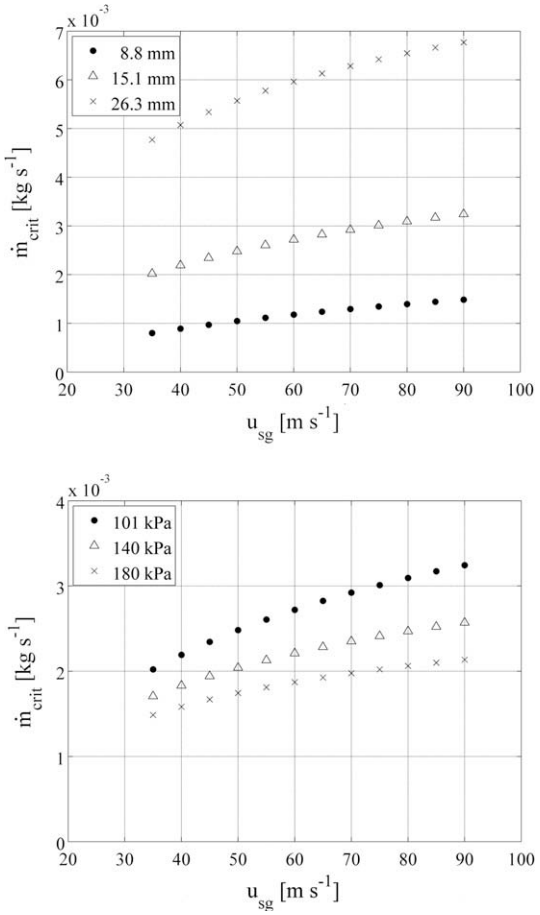

Fig. 8. Critical film flow rates, from model. (Top) Dependence on gas superficial velocity and tube diameter, 101 kPa absolute pressure. (Bottom) Dependence on gas superficial velocity and system pressure, 15.1 mm tube.

in that work. For a 25.4 mm tube (vertical upflow), critical film flow rates of between 0.0049 and 0.0060 kg s^{-1} (4.9–6.0 g s^{-1}) were estimated, weakly inverse with gas velocity. In a similar facility as that of Schadel, Asali (1984) found that the critical film flow rate in a 22.9 mm tube was approximately 5.6 g s^{-1} and not a strong function of gas velocity.

These results are in reasonable agreement with the present model that predicts $\dot{m}_{crit}$ of 4.8–6.8 g s^{-1} for the 26.3 mm tube, although there is not agreement regarding the effect of gas flow on critical liquid flow. This discrepancy may come from the different geometries (vertical upflow vs. horizontal), estimation technique (from entrainment data vs. from film model), or due to the gas density effect noted above. Additional experimental data regarding entrainment and critical film flow rate (particularly as functions of system pressure and gas flow rate) in horizontal geometry, or base film thickness measurements in vertical upflow, would be advisable to provide better comparisons.

7. Summary

- Base film thickness is inversely related to gas flow and increases with increasing liquid flow. At high gas flow rates, the dependence on liquid flow becomes small.
- Asymmetry shows similar gross trends as average base film thickness, with a dominant inverse gas flow rate effect and small liquid flow rate effect that is most significant at low gas flow rates.
- Film thickness and asymmetry both increase with increasing diameter, but the dependencies are less than linear.
- For the air–water–PVC combination, base film thickness is well-predicted by a roughness model that assumes a constant ratio of rough-tube and smooth-tube friction factors.
- Asymmetry is well-predicted by a modified Froude number that depends on gas mass flux and the correlated base film thickness.
- The film thickness model can also be used to estimate the critical liquid flow rate; these results are in fair agreement with those using entrainment measurements.

Acknowledgements

The authors appreciate the financial support for the data acquisition portion of this project provided by the Petroleum Research Fund and the National Science Foundation under Award No. CTS-0134510. Any opinions, findings, and conclusions or recommendations expressed in this material are those of the authors and do not necessarily reflect the views of the National Science Foundation.

References

Anderson, R.J., Russell, T.W.F., 1970. Film formation in two-phase annular flow. AIChE Journal 16 (4), 626–633.
Asali, J.C., 1984. Entrainment in vertical gas–liquid annular flows. Ph.D. Thesis, University of Illinois at Urbana-Champaign, Urbana, IL.
Butterworth, D., 1972. Air–water annular flow in a horizontal tube. Progress in Heat and Mass Transfer 6, 235–251.
Fukano, T., Ousaka, A., 1989. Prediction of the circumferential distribution of film thickness in horizontal and near-horizontal gas–liquid annular flows. International Journal of Multiphase Flow 150 (3), 403–419.

Hewitt, G.F., Jayanti, S., Hope, C.B., 1990. Structure of thin liquid films in gas–liquid horizontal flow. International Journal of Multiphase Flow 160 (6), 951–957.
Hurlburt, E.T., Newell, T.A., 2000. Prediction of the circumferential film thickness distribution in horizontal annular gas–liquid flow. Journal of Fluids Engineering 122, 1–7.
Hurlburt, E.T., Fore, L.B., Bauer, R.C., 2006. A two zone interfacial shear stress and liquid film velocity model for vertical annular two-phase flow. In: Proceedings of the ASME Fluids Engineering Division Summer Meeting 2006, vol. 2, Miami, FL, USA, pp. 677–684.
Jayanti, S., Hewitt, G.F., White, S.P., 1990. Time-dependent behavior of the liquid film in horizontal annular flow. International Journal of Multiphase Flow 160 (6), 1097–1116.
Laurinat, J.E., Hanratty, T.J., Jepson, W.P., 1985. Film thickness distribution for gas–liquid annular flow in a horizontal pipe. Physicochemical Hydrodynamics 6 (1 and 2), 179–195.
Lin, T.F., Jones, O.C., Lahey, R.T., Block, R.C., Murase, M., 1985. Film thickness measurements and modelling in horizontal annular flows. Physicochemical Hydrodynamics 60 (1/2), 197–206.
Okada, O., Fujita, H., 1990. Experimental studies of annular-mist flow in the non-equilibrium region of a long horizontal pipe (comparison between the mixing methods by a nozzle and a porous wall). FED – Advances in Gas–Liquid Flows 99, 57–64.
Pletcher, R.H., McManus Jr., H.N., 1965. The fluid dynamics of three dimensional liquid films with free surface shear: a finite difference approach. In: Proceedings of the 9th Mid-Western Conference on Mechanics (Developments in Mechanics), vol. 3, pp. 305–318.
Rodríguez, D.J., 2004. Characterization of bubble entrainment, interfacial roughness and the sliding bubble mechanism in horizontal annular flow. Ph.D. Thesis, University of Wisconsin-Madison, Madison, WI, USA.
Rodríguez, D.J., Shedd, T.A., 2004. Cross-sectional imaging of the liquid film in horizontal two-phase annular flow. In: 2004 ASME Heat Transfer/Fluids Engineering Summer Conference, Charlotte, NC, July, Paper 56445.
Schadel, S., 1988. Atomization and deposition rates in vertical annular two-phase flow. Ph.D. Thesis, University of Illinois at Urbana-Champaign, Urbana, Illinois.
Schubring, D., Shedd, T.A., 2008. Wave behavior in horizontal annular air–water flow. International Journal of Multiphase Flow 340 (7), 636–646.
Schubring, D., Shedd, T.A., 2009. Prediction of wall shear for horizontal annular air–water flow. International Journal of Heat and Mass Transfer 51 (1–2), 200–209.
Shedd, T.A., Newell, T.A., 1998. Automated optical liquid film thickness measurement method. Review of Scientific Instruments 690 (12), 4205–4213.
Sutharshan, B., Kawaji, M., Ousaka, A., 1995. Measurement of circumferential and axial liquid film velocities in horizontal annular flow. International Journal of Multiphase Flow 210 (2), 193–206.
Wallis, G.B., 1969. One-dimensional Two-phase Flow. McGraw-Hill, Inc., New York.
Whalley, P.B., 1987. Boiling Condensation and Gas–Liquid Flow. Clarendon Press, Oxford.